OPTICAL AND DIELECTRIC CHARACTERIZATION OF PVA CAPPED ZnSe NANORODS

K. S. Ojha*, A. K. Shrivastav

Department of Physics, National Institute of Technology Raipur (C. G.), India;
e-mail: kspectra12@yahoo.co.in

PVA passivated ZnSe nanorods have been synthesized using the solvothermal method. XRD analysis of the synthesized nanorods validates the cubic zinc blende structure with average particle size of 14 nm, and SEM analysis confirms the formation of rods having a wide range of lengths. A twin nanorod along with a typical nanostructure of rods has been observed in SEM micrographs. The optical characterization of the synthesized nanorods has been made using UV-Vis and photoluminescence spectroscopy. An energy gap of 3.89 eV has been observed, which is blue shifted from the bulk ZnSe. The dielectric study of ZnSe nanorods has been also made and reported.

Keywords: *ZnSe nanorod, solvothermal method, X-ray difraction, scanning electron microscopy, PL spectra, dielectric properties.*

ОПТИЧЕСКАЯ И ДИЭЛЕКТРИЧЕСКАЯ ХАРАКТЕРИСТИКА НАНОСТЕРЖНЕЙ ZnSe С ПЛЕНОЧНЫМ ПОКРЫТИЕМ

K. S. Ojha*, A. K. Shrivastav

УДК 539.261;535.37;620.3

Национальный технологический институт Раипур, Индия;
e-mail: kspectra12@yahoo.co.in

(Поступила 24 июля 2018)

Пассивированные ПВА наностержни ZnSe синтезированы с использованием сольвотермального метода. Рентгеноструктурный анализ синтезированных наностержней подтверждает характерную для цинковой обманки кубическую структуру со средним размером частиц 14 нм, исследования с помощью растровой электронной микроскопии (РЭМ) свидетельствуют об образовании стержней с большим диапазоном длин. На РЭМ-изображениях наряду с обычными стержневыми наноструктурами наблюдаются сдвоенные наностержни. Оптические характеристики синтезированных наностержней получены с использованием УФ-видимой и фотолюминесцентной спектроскопии. Запрещенная зона шириной 3.89 эВ смещена в синюю область спектра относительно положения указанной зоны в объемном образце ZnSe. Проведены исследования диэлектрических свойств наностержней ZnSe.

Ключевые слова: *наностержень ZnSe, сольвотермальный метод, рентгеноструктурный анализ, растровая электронная микроскопия, люминесценция, диэлектрические свойства.*

Introduction. Among various chalcogenides, ZnSe is one of the important II-VI semiconductors. The various forms of ZnSe at nanoscale level are of keen interest due to their vast applications in nanodevices. These various forms of ZnSe nanostructures have been synthesized by using different physical as well as chemical approaches, and their structural, optical, and electrical properties have been investigated by several workers [1–7]. The unique properties of these nanostructures are being used in a variety of device functionalities and have been demonstrated in light emitting diodes [8], single-electron transistors [9], and different quantum dot geometry dependent junctions [10]. Very few works have been carried out to synthe-

size one-dimensional ZnSe nanostructures such as nanowires, nanorods, nanotubes, etc. Panda et al. [11] synthesized ultrathin as well as uniform ZnSe nanorods of length 4.5 nm and nanowires of length in the range 100–200 nm having the same 1.3 nm diameter. The synthesized nanorods and nanowires are characterized spectroscopically, and their uniformity has been confirmed. Thermally treated wurtzite ZnSe nanowires, of length tens of microns and diameter in the range of 15–20 nm, have been synthesized by Xiong et al. [12], and three luminescence peaks lying at 435, 462, and 587 nm has been reported. Fanfair and Korgel [13] developed ZnSe nanowires using the solution−liquid−solid mechanism in the presence of trioctylamine and trioctylphosphine oxide and reported that the nanowires produced in trioctylamine have short branches predominantly growing in the (112) direction, whereas nanowires produced in trioctylphosphine oxide have no branches and grow in the (111) direction. Dong et. al. [14] synthesized colloidal homo branched ZnSe nanowires using solution-liquid-solid growth process in combination with a sequential seeding strategy and reported that the crystalline branches grow epitaxially from the backbone. Yim et. al. [15] prepared ZnSe nanowires of large aspect ratio and length up to a few millimeters using the vapor transport technique. Mn-doped ZnSe nanowires 2–3 μm long and 80 nm thick were successfully prepared using hydrothermal method by Han et al. [16], and a sharp absorption peak lying at 360 nm along with two luminescence bands lying at 432 and 580 nm has been reported. Zhang and Yang [17] synthesized 75 nm thick and more than 10 μm long twinned cubic ZnSe nanowires using the solvothermal process and reported that the nanowires show strong emissions of both phases of ZnSe. ZnSe nanowires of high quality and having diameters in the range 15–20 nm with length 4–10 μm have been synthesized by Petchsang et al. [18] using a solution–liquid–solid growth technique. Cubic and ultrathin ZnSe nanorods with improved photocatalytic activities have been synthesized by Yao et al. [19] using the reaction between selenium and zinc oleate. High-quality ZnSe nanowires are prepared by Wang et al. [20] through an Ag_2Se-catalyzed growth mechanism, and a significant blue shift in the band gap of ZnSe nanowire in comparison with the bulk is observed.

The use of organic polymers for the synthesis of semiconductor nanostructures is a prominent method because the polymer matrices provide good processability and solubility. Among other organic polymers, polyvinyl alcohol (PVA) is an optically transparent, hydrophilic, biodegradable, biocompatible as well as nontoxic polymer and has better film forming capacity. The aqueous solubility and high viscosity of PVA matrix prevents particles from agglomeration and thus is helpful in controlling the growth of ZnSe nanorods. Since the PVA matrix also protects it from photo-oxidation, ZnSe nanorods implanted in the PVA matrix is a good candidate material for their-ready-use applications in optical devices. The optical and dielectric properties of ZnSe nanorods embedded in the PVA matrix have not been studied extensively. Therefore, in the present study, ZnSe nanorods in the PVA matrix have been synthesized via the solvothermal process, and their structural and optical and dielectric properties have been investigated.

Materials and method. The ZnSe nanorods are synthesized via the solvothermal process adopted by Jana et al. [4]. The zinc chloride ($ZnCl_2$), selenium oxide (SeO_2), and organic polymer PVA are used as raw materials, and all the materials used are of purity about 99%. A thick and transparent mixture of PVA is prepared by mixing 2 g of PVA in 100 ml of distilled water under stable stirring at 90°C for 2 h. A 0.2 mM portion of $ZnCl_2$ is mixed with 25% of ammonia solution under continuous stirring to prepare a solution of 20 mL, and then 0.2 mM of SeO_2 along with 20 mL of PVA solution are added to the prepared mixed solution of $ZnCl_2$ and ammonia. After 1 h of stirring, the resulting reaction mixture is transferred into a stainless autoclave and then sealed. The sealed autoclave is kept at 240°C for 2 h. After 2 h, the product contained in the autoclave is chilled automatically to room temperature and then centrifuged to find the yield. The final yield is washed with ethanol and distilled water several times and then dried in vacuum at 70°C. The synthesized products are used for further characterization.

Results and discussion. *Structural study.* The structural properties of ZnSe nanorods embedded in the PVA matrix have been investigated using a Rigaku mini flex X-ray diffractometer with CuK_α radiation (1.5418 Å). The diffraction pattern, recorded in the range of 2θ from 20° to 80° at the scanning speed of 0.02°/min, is presented in Fig. 1. The diffraction peaks observed at 27.18, 29.58, 45.16, 49.18, 53.46, 65.80, and 72.60° are indexed as (111), (101), (220), (103), (311), (400), and (331) reflection planes of cubic zinc blende ZnSe nanorods, respectively. The diffraction pattern also confirms that no impurity is present in the synthesized nanorods. The sharp and strong peaks observed in the pattern signify the crystalline nature of the ZnSe nanorods. The crystalline nature of the synthesized nanorods is due to the decrease in number of hydrogen bonds formed between the layers of the PVA matrix upon the incorporation of ZnSe into PVA [21, 22]. This signifies that the amorphous PVA acts as a stabilizer and controls the growth of the nanorods. The mean crystallite size is obtained from Scherrer's formula given by

$$D = k\lambda/\beta\cos\theta,$$

where D, k, λ, β, and θ represent the average crystallite size, particle shape factor, wavelength of X-ray, full width at half maximum (FWHM) intensity, and Bragg's angle, respectively. The crystallite size calculated from the XRD pattern corresponding to the (111) reflection peak is found to be 14 nm.

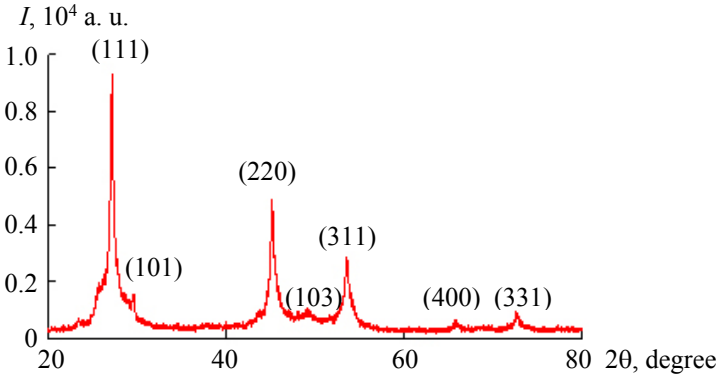

Fig. 1. XRD pattern of ZnSe nanorods.

Morphological study. The morphology of the synthesized ZnSe nanorods has been studied using a JEOL-JSM6700 scanning electron microscope operating 15 kV, and the micrographs are shown in Fig. 2 at different magnifications. The micrographs confirm the formation of nanorods having lengths ranging from 9–105 nm as a result of the solvothermal technique used. A twin nanorod shown by red arrow along with a typical structure of nanorods shown by white arrows has been synthesized and is shown Fig. 2b. The micrographs also reveal that the synthesized rods are straight without any nanoparticle impurities.

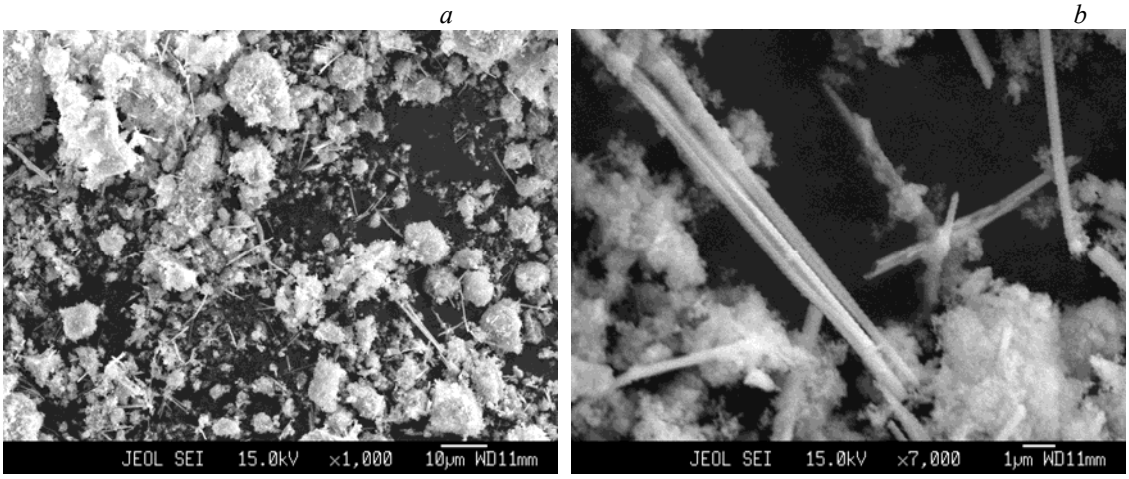

Fig. 2. Scanning electron micrographs of ZnSe nanorod at various magnifications.

UV-visible study. The room temperature optical study of the synthesized ZnSe nanorods has been made using a LAMBDA 35 spectrophotometer (Perkin Elmer) by using UV-Vis spectroscopy. The observed spectrum, represented in Fig. 3a, reveals a strong absorption peak at 372.3 nm and is in close agreement with that reported by Ahamed et al. [23]. The energy band gap of ZnSe nanowire is determined by extrapolating the linear region of the graph plotted between $(\alpha h\nu)^2$ versus $h\nu$ and is displayed in Fig. 3b. An energy bandgap of 3.89 eV has been observed, which is shifted towards shorter wavelengths (~1.19 eV) in comparison with the energy gap of bulk ZnSe (E_g ~ 2.7 eV) due to the size reduction effect in the presence of PVA matrix.

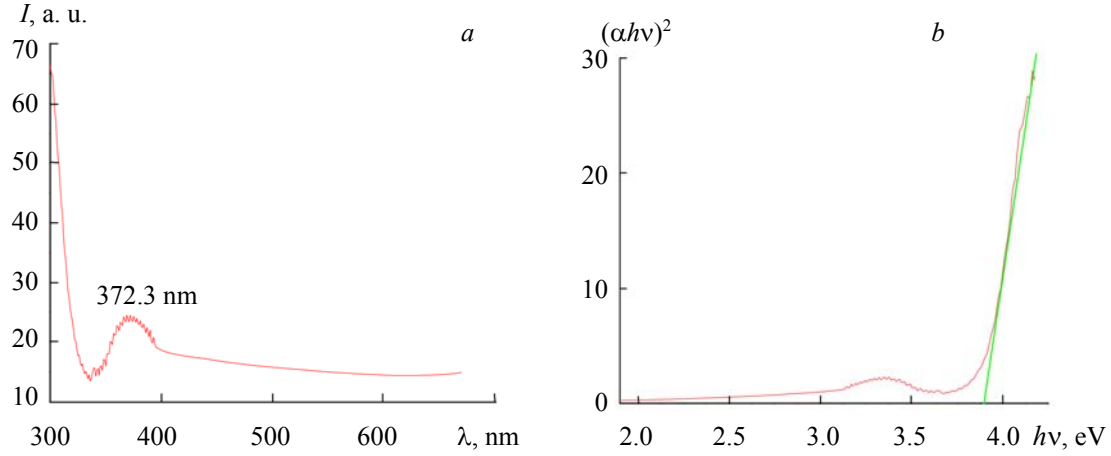

Fig. 3. UV-vis absorption spectrum (a) and Tauc plot of ZnSe nanorods (b).

Photoluminescence study. The photoluminescence technique is a highly sensitive and non-destructive technique. Therefore it is widely used to examine the photon related properties of active sites of ZnSe nanorods. The PL characterization has been done by using a PerkinElmer luminescent spectrometer LS-55.

The photoluminescence emission spectrum of ZnSe nanorods is shown in Fig. 4. From figure a sharp peak lying at 231 nm is clearly observed, which is also in close agreement with that reported by Ahamed et al. [23]. The figure also reveals that the photoluminescence peak moves in the direction of shorter wavelengths due to the quantum confinement effect and originates due to the recombination of a hole induced by a photon and a particular defect charge state.

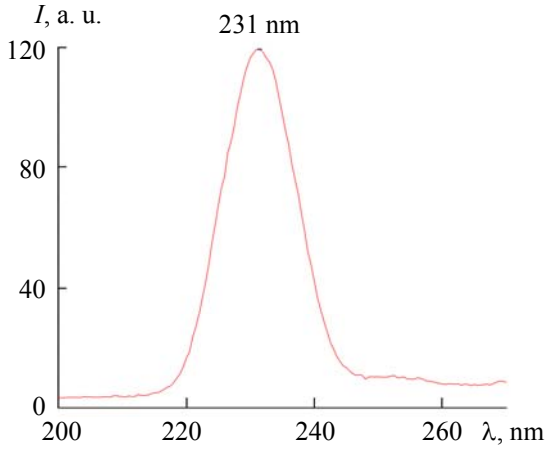

Fig. 4. Photoluminescence spectrum of ZnSe nanorods.

Dielectric study. The variation of dielectric loss of PVA capped ZnSe nanorods as a function of frequency ranging from 1 kHz to 1.5 MHz at various temperatures is depicted in Fig 5a. The dielectric loss shows high values at smaller frequencies (<100 kHz) for all temperatures, which is possible due to the interfacial polarization. The values of dielectric loss at frequencies greater than 100 kHz become almost constant and can be explained on the basis of the Maxwell-Wagner-Sillars effect in which electrical heterogeneity induces inertia due to dipoles [24]. The dielectric loss values also increase with increase in temperature in the low frequency region. The variation of dielectric constant of the synthesized ZnSe nanorods as a function of frequencies ranging from 500 kHz to 5 MHz at various temperatures is depicted in Fig. 5b, which shows that in the low frequency region, a decrease in the value of dielectric constant is observed as the frequency increases, while in the high frequency region it becomes constant for all temperatures. A fast decrease in the values of dielectric constant has been observed in the frequency regime less than 1 MHz while in the frequency region from 1 to 3.25 MHz the decrease become slower. Koop's theory and the Maxwell-Wagner

two layers models [25] can be used to explain the variations observed in the dielectric constant. In the low frequency regime, the induced space charge polarization due to the oppositely aligned space charge with respect to the applied field enhances the values of the dielectric constant. In the higher frequency regime, the rotation dielectric polarization induced by self-aligned dipoles formed by positive and negative charges in the presence of the applied field and the space charge polarization increases due to the small volume of the particle as well as lagging of species responsible for both polarizations [26]. It is also obvious from Fig. 5b that the dielectric constant value increases with increase in temperature and is in close agreement with Debye relaxation [27].

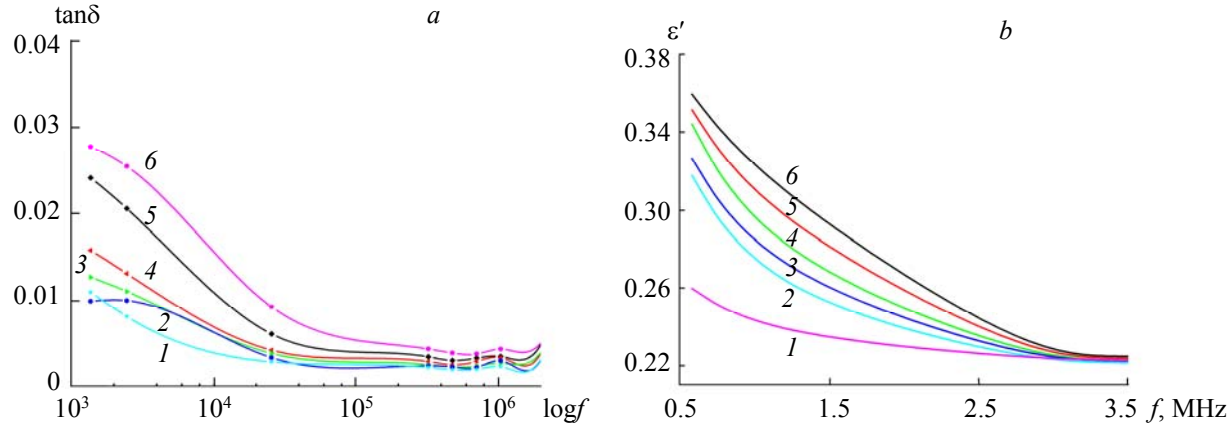

Fig. 5. Variation of dielectric loss (a) and dielectric constant (b) of ZnSe nanorod with frequencies at various temperatures: 30 (1), 40 (2), 50 (3), 60 (4), 70 (5), and 80 °C (6).

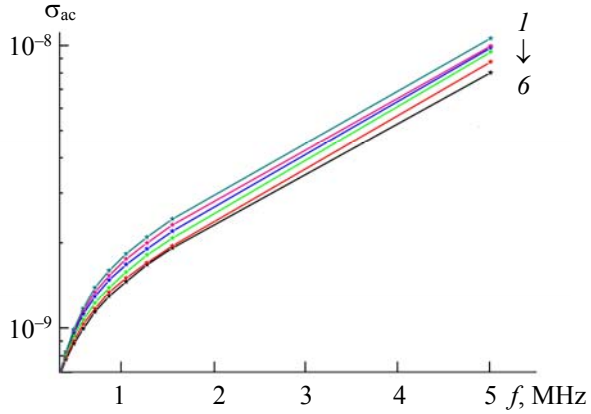

Fig. 6. Variation of AC conductivity of ZnSe nanorod with frequency at different temperatures: 30 (1), 40 (2), 50 (3), 60 (4), 70 (5), and 80 °C (6).

The frequency dependent behavior of AC conductivity of PVA capped ZnSe nanorods at various temperatures is represented in Fig. 6. The figure implies that a frequency regime less than 1 MHz, there is a slight increase in the conductivity, but at a frequency larger than 1MHz, the conductivity increases abruptly for all temperatures due to small polaron. According to the Maxwell–Wagner and Koop's theory [25], the increase in conductivity at frequencies less than 1 MHz is attributed to electron hopping, while at frequencies larger than 1 MHz, the charge carrier mobility increases with increasing charge carrier hopping, and hence the conductivity increases. A decrease in conductivity with rise in temperature has been observed in Fig. 6 and is attributed to the enlargement of particle size.

Conclusion. Cubic zinc blende PVA capped ZnSe nanorods, of lengths ranging from 9 to 105 nm and diameter of a few nanometers, have been synthesized using the solvothermal process. The band gap energy obtained from UV-Vis spectroscopy is found to be 3.89 eV, and a blue shift relative to bulk samples is observed in the absorption edge. The origin of the emission peak centered at 231 nm has been discussed. The dielectric loss and dielectric constant value decrease, while the AC conductivity increase with increase in frequency. ZnSe nanorods incorporated in the PVA matrix have enormous applications in nanoelectronics and nanophotonics. Cubic zinc blende-structured ZnSe nanorods are being used in manufacturing blue laser diodes, light emitting diodes, solar cells, IR optical windows, etc. In addition to these, the high third-order nonlinearity of one-dimensional ZnSe nanostructures makes them suitable candidates for optical switches, digital signal restoration, optical storage media, and optical limiters.

REFERENCES

1. L. S. Li, N. Pradhan, Y. Wang, X. Peng, *Nano Lett*., **4**, No. 11, 2261–2264 (2004).
2. M. A. Rafea, *J. Mater. Sci.: Mater. Electron*., **18**, 415–420 (2007).
3. A. C. Deshpande, S. B. Singh, M. K. Abyaneh, R. Pasricha, S. K. Kulkarni, *Mater. Lett*., **62**, 3803–3805 (2008).
4. S. Jana, I. C. Baek, M. A. Lim, S. I. Seok, *J. Colloid Interface Sci*., **322**, 473–477 (2008).
5. J. Archana, M. Navaneethan, S. Ponnusamy, Y. Hayakawa, C. Muthamizhchelvan, *Appl. Surf. Sci*., **257**, 7699–7703 (2011).
6. Ch. Rajesh, C. Phadnis, K. G. Sonawane, S. Mahamuni, *J. Exp. Nanosci*., **10**, No. 14, 1082–1092 (2015).
7. N. K. Nasab, A. R. Dehnad, H. Salimizand, D. Taherzadeh, D. Prakash, K. D. Verma, M. Darroudi, *Ceram. Int*., **42**, 12115–12118 (2016).
8. M. S. Gudiksen, L. J. Lauhon, J. Wang, D. C. Smith, C. M. Leiber, *Nature*, **415**, 617–620 (2002).
9. C. Thelander, T. Martensson, M. T. Bjork, B. J. Ohlsson, M. W. Larsson, L. R. Wallenberg, L. Samuelson, *Appl. Phys. Lett*., **83**, 2052–2054 (2003).
10. C. Yang, Z. H. Zhong, C. M. Lieber, *Science*, **310**, 1304–1307 (2005).
11. A. B. Panda, S. Acharya, S. Efrima, *Adv. Mater*., **17**, No. 20, 2471–2474 (2005).
12. S. L. Xiong, J. Shen, Q. Xie, Y. Q. Gao, Q. Tang, Y. T. Qian, *Adv. Funct. Mater*., **15**, No. 11, 1787–1792 (2005).
13. D. D. Fanfair, B. A. Korgel, Chem. Mater., **19**, No. 20, 4943–4948 (2007).
14. A. Dong, R. Tang, W. E. Buhro, *J. Am. Chem. Soc*., **129**, No. 40, 12254–12262 (2007).
15. J. W. L. Yim, D. Chen, G. F. Brown, J. Wu, *Nano Res*., **2**, 931–937 (2009).
16. D. Han, C. Song, X. Li, *J. Nanomater*., **290763** (1–4) (**2010**); doi:10.1155/2010/290763.
17. L. Zhang, H. Yang, *App. Phys. A: Mater. Sci. Proc*., **98**, No. 4, 801–810 (2010).
18. N. Petchsang, L. Shapoval, F. Vietmeyer, Y. Yu, J. H. Hodak, I.-M. Tang, T. H. Kosel, M. Kuno, *Nanoscale*, **3**, No. 8, 3145–3151 (2011).
19. T. Yao, Q. Zhao, Z. Qiao, F. Peng, H. Wang, H. Yu, C. Chi, J. Yang, *Chem. A Eur. J.* **17**, No. 31, 8663–8670 (2011).
20. J. Wang, H. Feng, W. Fan, K. Chen, Q. Yang, *Adv. Mater. Phys. Chem*., **3**, 289–294 (2013).
21. W. E. Mahmoud, H. M. El-Mallah, *J. Phys. D: Appl. Phys*., **42**, 1–5 (2009).
22. M. Sharma, S. K. Tripathi, *J. Phys. Chem. Solids*, **73**, 1075–1081 (2012).
23. A. J. Ahamed, K. Ramar, P. V. Kumar, *J. Nanosci. Nanotechnol*., **2**, No. 3, 148–150 (2016).
24. H. Y. Chang, C. T. Lin, S. J. Chiu, *Desalination*, **233**, 137–146 (2008).
25. C. G. Koops, *Phys. Rev.*, **83**, 121–124 (1951).
26. G. Yellaiah, T. Shekharam, K. Hadasa, M. Nagabhushanam, *J. Alloys. Compd.*, **609**, 192–200 (2014).
27. H. Demiryont, *J. Appl. Phys*., **49**, 2898–2904 (1978).